

DOPD: A Dynamic PD-Disaggregation Architecture for Maximizing Goodput in LLM Inference Serving

Junhan Liao, Minxian Xu, *Senior Member, IEEE*, Wanyi Zheng, Yan Wang, *Member, IEEE*, Kejiang Ye, *Senior Member, IEEE*, Rajkumar Buyya, *Fellow, IEEE*, Chengzhong Xu, *Fellow, IEEE*

Abstract—To meet strict Service-Level Objectives (SLOs), contemporary Large Language Models (LLMs) decouple the prefill and decoding stages and place them on separate GPUs to mitigate the distinct bottlenecks inherent to each phase. However, the heterogeneity of LLM workloads causes producer-consumer imbalance between the two instance types in such disaggregated architecture. To address this problem, we propose DOPD (Dynamic Optimal Prefill/Decoding), a dynamic LLM inference system that adjusts instance allocations to achieve an optimal prefill-to-decoding (P/D) ratio based on real-time load monitoring. Combined with an appropriate request-scheduling policy, DOPD effectively resolves imbalances between prefill and decoding instances and mitigates resource allocation mismatches due to mixed-length requests under high concurrency. Experimental evaluations show that, compared with vLLM and DistServe (representative aggregation-based and disaggregation-based approaches), DOPD improves overall system goodput by up to 1.5 \times , decreases P90 time-to-first-token (TTFT) by up to 67.5%, and decreases P90 time-per-output-token (TPOT) by up to 22.8%. Furthermore, our dynamic P/D adjustment technique performs proactive reconfiguration based on historical load, achieving over 99% SLOs attainment while using less additional resources.

Index Terms—Large Language Models, LLM inference serving, dynamic, efficiency, resource management.

I. INTRODUCTION

SINCE Transformer-based [1] LLMs have demonstrated powerful capabilities in natural language processing [2], an increasing number of researchers have pursued deeper investigations [3] [4] to make LLMs such as GPT-5 [5], LLaMa-4 [6] more capable. Concurrently, the deployment of LLMs has become increasingly pervasive across a wide range of industries/commercial applications such as advanced Bing search engine [7], Google’s AI assistant [8], AI code editor [9], log-based fault diagnosis [10]. However, more powerful

J. Liao, M. Xu and K. Ye are with Shenzhen Institutes of Advanced Technology, Chinese Academy of Sciences, Shenzhen, China.

W. Zheng is with Southern University of Science and Technology, and is also a joint-training student at the Shenzhen Institutes of Advanced Technology, Chinese Academy of Sciences, Shenzhen, China.

Yan Wang is with the College of Computer Science, Inner Mongolia University, Inner Mongolia, China.

R. Buyya is with the Quantum Cloud Computing and Distributed Systems (qCLOUDS) Laboratory, School of Computing and Information Systems, the University of Melbourne, Melbourne, Australia.

C. Xu is with State Key Lab of IOTSC, University of Macau, Macau, China.

This work is supported by National Natural Science Foundation of China under Grant 62572462, Guangdong Basic and Applied Basic Research Foundation (No. 2024A1515010251, 2023B1515130002), Key Research and Development and Technology Transfer Program of Inner Mongolia Autonomous Region (2025YFHH0110) and Shenzhen Science and Technology Program under Grant JCYJ20240813155810014.

M. Xu is the corresponding author.

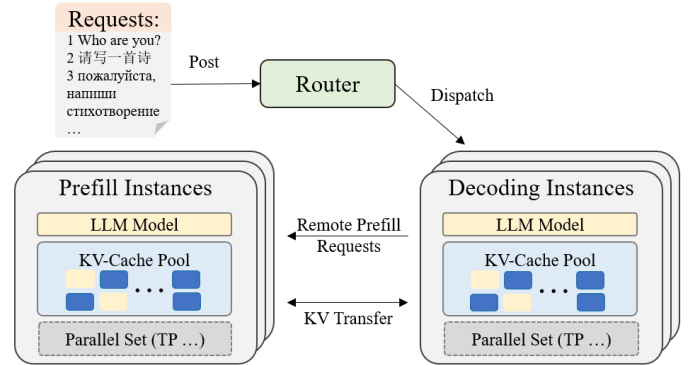


Figure 1: Prefill-decoding disaggregation diagram.

models often possess extremely large parameter counts. For example, kimi-k2 [11] contains over 1 trillion parameters. As model parameter counts grow, the computational and storage costs of inference increase substantially. Consequently, LLMs often run on expensive, energy-intensive GPUs [12].

Optimizing LLM inference to reduce these costs has therefore become a major research focus [13] [14]. Both academic and industrial efforts have proposed several techniques [15]. For example, Key-Value (KV) caching caches historical KV tensors to avoid redundant recomputation. FlashAttention [16] reduces GPU memory-access overhead when computing attention. Mixture-of-Experts (MoE) [17] architectures substantially expand model capacity and improve performance without proportionally increasing computation. Because mainstream LLMs are based on the Transformer architecture, current generative LLMs are typically autoregressive which means a single request each output token is produced sequentially during forward inference. Based on the per-token computation and KV caching, LLM inference can be partitioned into two phases: the prefill phase and the decoding phase. The prefill phase produces the first output token by processing the entire input sequence. This requires computing the KV tensors for the full prompt and induces a heavy compute bottleneck on the GPU. By contrast, the decoding phase generates subsequent tokens autoregressively. At each decoding step only the most recently generated token is used as input and, with KV Caching, only the per-step Query/Key/Value for the new token must be computed, yielding a relatively light compute load. To improve throughput, decoding-phase requests are commonly batched. However, as inference proceeds the accumulated KV-cache grows, and batched decoding processing must read increasingly large KV tensors from GPU memory, which

for large batch sizes induces a severe memory-bandwidth bottleneck.

Prior works such as DistServe [18] and SplitWise [19] propose deploying the prefill and decoding phases on separate devices to avoid the resource contention that arises when mixed-phase requests are processed on the same device. Figure 1 illustrates the overall architecture of such Prefill-Decoding-Disaggregation (PD-Disaggregation) systems, which are organized into P-instances (perform only prefill inference) and D-instances (perform only decoding inference). By placing these stages on distinct devices, the compute-bound prefill bottleneck and the memory-bound decoding bottleneck can be mitigated independently. However, PD-Disaggregation introduces an additional producer-consumer imbalance. In this architecture P-instances act as producers that execute prefill inference and produce prefill-completed requests, while D-instances act as consumers that consume those prefill-completed requests and perform the subsequent Decoding inference. When the production capacity of the P-instances and the consumption capacity of the D-instances are imbalanced, substantial resource underutilization or overload can occur. Only a suitable configuration of P-instances and D-instances can eliminate this imbalance. Because LLM inference request lengths vary, the optimal configuration changes over time and static deployments remain susceptible to producer-consumer imbalance. Reconfiguring resource allocation incurs substantial time cost, therefore mitigating the short term mismatch between static PD-Disaggregation deployments and mixed-length request traffic remains a challenging problem.

To address these challenges, we tackle the problem of dynamically adjusting the P/D ratio in a PD-Disaggregation deployment to improve goodput. Concretely, we (i) derive a principled method to compute an optimal P/D ratio for a given load regime, (ii) apply intelligent scheduling to mitigate the short term resource mismatch caused by mixed-length requests and improve the effectiveness of systems in high-load scenarios, and (iii) leverage the monitoring data we re-evaluate the system P/D ratio and decide whether the current configuration remains optimal or requires elastic scaling of P-instances and D-instances. Our contributions are as follows:

- We design DOPD, an intelligent and dynamic LLM-inference framework that continuously tunes the number and configuration of P-instances and D-instances.
- We present a comprehensive system model and in-depth analysis of PD-Disaggregation, identifying the key challenges faced by disaggregated inference architectures.
- We propose an optimal P/D ratio calculation method that integrates device-level and workload-level factors, and we design an intelligent, length-aware request-scheduling algorithm to mitigate resource mismatch caused by mixed-length inference workloads.
- We perform extensive experiments demonstrating that DOPD substantially increases system goodput ($1.5\times$) and the SLO attainment (from 80.8% to 99.4%) under realistic production traces.

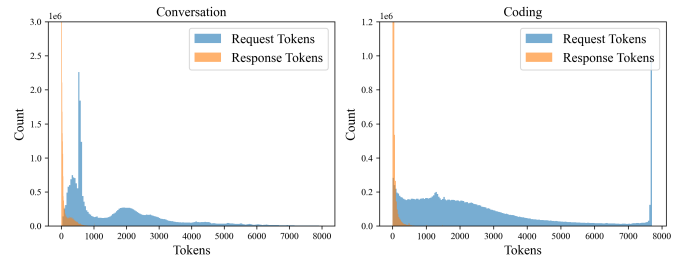


Figure 2: The input/output length of request tokens in Microsoft Azure traces dataset.

II. MOTIVATION

This section summarizes the issues we observe in existing PD-Disaggregation systems and motivates our design choices.

A. Motivation: Difficulty of Predicting LLM Inference Workloads

Modern LLM inference workloads are highly heterogeneous and nonstationary. Individual user requests exhibit large variability in input and output sequence lengths, which makes accurate load prediction challenging. Figure 2 illustrates the input/output length distributions from a production trace (Microsoft Azure traces)¹. These traces were collected from real user interactions with LLM services and exhibit wide length variance, lack clear periodic patterns, and frequently contain sudden bursts. Such characteristics render many traditional prediction methods ineffective, yet accurate short-term forecasts of inference load are essential for prudent resource pre-allocation. For LLMs deployments, knowing the near-term inference load in advance enables proactive adjustment of instance allocations, which is critical for preventing resource waste and avoiding overload in PD-Disaggregation systems.

To mitigate this challenge, applying a multiplicative scaling (correction) factor can be effective. By comparing the most recent forecast with observed measurements and adjusting future forecasts accordingly, the scaling factor attenuates systematic bias between predicted and actual values and keeps prediction error within a bounded, small range.

B. Motivation: P/D Ratio Critically Impacts PD-Disaggregation Performance

Under PD-Disaggregation, a P-instance performs the prefill inference and transmits both the request metadata and the computed KV-cache to a D-instance. Once a D-instance receives the full KV-cache it proceeds with decoding inference. When all requests follow this PD-Disaggregation flow, P-instances and D-instances form a producer-consumer pair. Each prefill inference (produced by a P-instance) generates one decoding request, and each decoding inference (consumed by a D-instance) consumes one such request. If the production capacity of P-instances does not match the consumption capacity of D-instances, an imbalance arises that causes either overload or underutilization on one side, substantially degrading average throughput and degrading overall user experience.

¹<https://github.com/Azure/AzurePublicDataset>

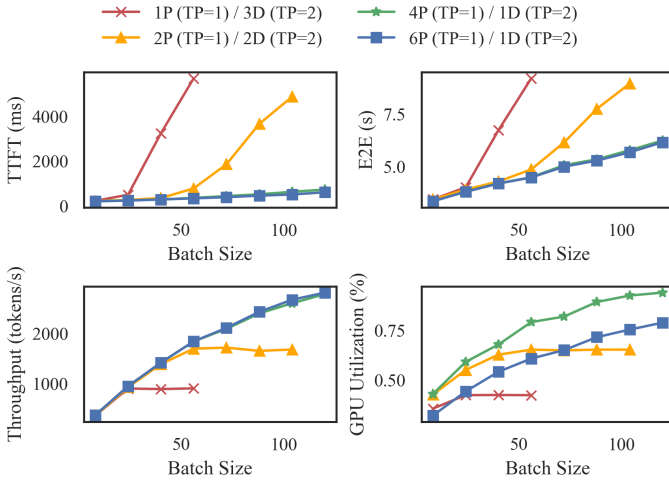


Figure 3: The experiment of different P/D ratio. The "2P (TP=1) / 2D (TP=2)" in picture represents a PD-Disaggregation deployment comprising 2 P-instances each deployed on a single GPU (tensor parallel size = 1) and 2 D-instances each deployed across two GPUs (tensor parallel size = 2). Some of the curves in the picture are incomplete because subsequent experiments are meaningless. For example, the configuration corresponding to the red curve cannot cope with a load exceeding a request concurrency of 50.

Figure 3 shows experimental results under different P/D ratios. The results reveal large performance differences across P/D ratios. A well-chosen P/D composition achieves 3.2 \times the throughput (as shown in Figure 3(c)) of a poorly chosen composition and increases average GPU utilization by 86.0% (as shown in Figure 3(d)), while reducing TTFT by 15.32 \times and end-to-end latency (E2E) by 1.04 \times . Hence, selecting an appropriate P/D ratio is critical for improving GPU utilization and overall inference performance.

Thus, to fully realize the benefits of PD-Disaggregation, a system should be capable of computing an optimal P/D ratio that comprehensively accounts for current load, model characteristics and device properties. It should then configure P-instances and D-instances accordingly so as to improve GPU utilization and the SLO attainment under the prevailing workload.

C. Motivation: Mixed-length Requests Undermine PD-Disaggregation

In LLM inference systems, the PD-Disaggregation architecture which separates prefill and decoding work onto different devices has emerged as an effective means to improve throughput and resource utilization. However, prior work [20], [21] and our observations show that when the workload is a mixture of requests with widely varying lengths, PD-Disaggregation can perform substantially worse than deployments in which all requests share a fixed length. The root cause is that different request lengths have different optimal allocations between prefill and decoding resources. Short requests tend to complete decoding quickly while consuming relatively little prefill capacity, whereas long requests require a higher proportion of prefill resources to sustain pipeline efficiency. If requests with

Table I: For different sequence lengths, we measure the single-run prefill inference latency and the single-step decoding inference latency at different concurrency, where cc refers to request concurrency in the system.

Sequence Length	$T_{prefill}$ (ms)	$T_{decoding}$ (ms)		
		cc = 104	cc = 200	cc = 248
100	36	28	45	47
200	46	31	46	49
700	125	33	47	53
1200	193	35	50	57
1700	269	37	53	61

very different lengths (e.g., 100 tokens and 1900 tokens) are mixed and a single global P/D ratio is chosen based on the mean length (e.g., 1000 tokens), the resulting static allocation typically cannot satisfy the local optima for both short and long requests simultaneously. In other words, the optimal P/D ratio is highly nonlinear and distribution-dependent with respect to request length. Static configurations based on average length of requests therefore produce either resource shortages or long queuing for subsets of requests, degrading overall throughput and tail latency and eroding the benefits of PD-Disaggregation.

At the same time, for extremely short requests whose prefill compute time is negligible, the KV-cache transfer latency between P-instances and D-instances becomes a nontrivial fraction of end-to-end latency. Table I reports, for a single H100 GPU [12] running an FP8-quantized Llama-70B-FP8 model, the per-request prefill time and the per-step decoding time (under maximum batching) for several sequence lengths. For example, a prefill for a prompt of length 100 tokens may take approximately 36ms, while a single decoding step at 248 batch size can take approximately 47ms. Even with NIXL's [22] efficient GPU-to-GPU transfers, KV-cache transmission can add on the order of 15-80ms depending on block fragmentation and count, rendering PD-Disaggregation uneconomical for such requests. In such cases, executing these ultra-short requests in-place (i.e., without remote prefill) typically produces negligible interference with other decoding work, whereas routing them through remote prefill incurs unnecessary KV-cache transfer overhead and increases TTFT. Hence, offloading all ultra-short requests to remote P-instances is often suboptimal.

These two observations motivate the need for length-aware scheduling and workload-aware adaptation. Designing scheduling policies that account for request-length heterogeneity is essential to improve the robustness and efficiency of practical inference systems under mixed workloads.

Motivated by the foregoing, we propose **DOPD**, a PD-Disaggregation framework that (i) produces accurate short-term forecasts of future load, (ii) computes the optimal P/D ratio for the current workload, (iii) leverages workload-aware request scheduling to mitigate the interference introduced by mixed-length requests in PD-Disaggregation under high concurrency, and (iv) dynamically scales the numbers of P-instances and D-instances according to the computed optimal P/D ratio. By reacting to complex and rapidly varying loads, DOPD maximizes goodput without under-provisioning

or over-provisioning GPU resources, reduces TPOT and end-to-end latency, and maintains excellent SLO attainment.

III. RELATED WORK

This section surveys recent techniques that mitigate interference between prefill and decoding requests and discusses their limitations.

A. Aggregation-based Approaches

Yu et al. propose Orca [23], which uses continuous batching (iteration-level batching and selective batching) applied to generation to mitigate interference from prefill requests within the same batch. Kwon et al. introduce vLLM [24], which separates prefill and decoding requests into different batches and provides optimized operators for the two request types to improve computational efficiency. Both approaches partially alleviate prefill-to-decoding interference, but long-context prefill requests can still delay fast decoding requests.

Agrawal et al. present Sarathi-Serve [25], introducing chunked-prefill and stall-free batching to split long prefill work into smaller chunks that can be interleaved with decoding work. Building on mixed-batch techniques, Kamath et al. propose POD-Attention [26], a kernel-level redesign of the attention operator that enables true prefill–decoding overlap on a single GPU by partitioning computation and memory resources at the streaming-multiprocessor level. In practice, POD-Attention further mitigates low decoding throughput and prefill resource domination, yet these methods exhibit stability limitations under high concurrency, long-context workloads, or strict TTFT requirements.

And some other works propose reducing prefill-phase computation to mitigate the interference caused by co-processing prefill and decoding requests, for example RadixAttention [27] and Native Sparse Attention [28]. However these approaches are not universally applicable and some may introduce accuracy degradation.

In summary, aggregation-based approaches flexible batching, chunked prefill, kernel-level attention redesign, and sparse-attention techniques yield tangible gains but rely on complex, hardware-dependent kernel implementations, introduce additional implementation or memory overheads, and may compromise accuracy in some regimes. More importantly, they do not fundamentally eliminate the conflict between prefill and decoding requests. By contrast, DOPD employs targeted, length-aware request scheduling to selectively separate or aggregate requests, achieving stronger SLO adherence while preserving high goodput.

B. Disaggregation-based Approaches

Zhong et al. formalize the cost of colocated execution in DistServe [18], demonstrating that colocating prefill and decoding causes strong interference and proposing fully decoupled deployments to improve goodput. Patel et al. build on PD-Disaggregation to present SplitWise [19], which maximizes computation–communication overlap via a hierarchical KV-cache transfer design and thereby reduces the impact of

Table II: Comparison of related work which is disaggregation-based Approach.

Approaches	Dynamic P/D	Efficient KV-cache Transfer	Optimal P/D
Zhong et al. [18]	×	×	×
Patel et al. [19]	×	✓	×
Qin et al. [29]	×	✓	×
Jin et al. [30]	✓	✓	×
Wu et al. [31]	✓	✓	×
Dynamo [32]	✓	✓	×
Our Work (DOPD)	✓	✓	✓

KV-cache transfer overhead. Similarly, Qin et al. propose Mooncake [29], a KV-cache–centric disaggregated architecture that optimizes prefill-to-decoding KV-cache migration via D2D/RDMA transport and KV-aware scheduling. However, these methods are largely static and do not support real-time dynamic adjustment of instance counts, which can lead to substantial resource waste and transient overloads under variable workloads.

Jin et al. propose PD-Serve [30], which constructs fine-grained P/D grouping by scenario so that requests with similar prefixes are processed within the same group, and which optimizes KV-cache transfer and encoding parallelism while supporting dynamic scaling. Likewise, Wu et al. propose Arrow [31], which designs adaptive scheduling and an elastic instance pool that dynamically adjusts P-instance and D-instance counts based on cluster metrics, improving robustness to bursts and fluctuations. More recently, NVIDIA released the Dynamo framework [32], which advocates prefill–decoding separation to enable tailored tensor parallel size and memory strategies and parallelism. Although these systems introduce dynamic expansion, they still fall short in selecting optimal P/D instance counts and configurations after scaling: achieving post-scale optimal P/D configurations remains difficult, often resulting in significant GPU idleness or overload.

A comparison of representative characteristics of prominent PD-Disaggregation studies is presented in Table II. In summary, the disaggregation-based of approaches decouple prefill and decoding and, on that basis, optimize KV-cache migration and transfer to overlap computation and communication (e.g., SplitWise’s hierarchical transfer), and introduce fine-grained grouping and elastic/adaptive scheduling (e.g., PD-Serve’s P/D grouping). These measures reduce direct resource contention between the two request types. But many early solutions lack support for real-time, fine-grained elastic scaling, causing resource waste or short-term overloads under fluctuating load. And even systems that support dynamic scaling still face the unresolved challenge of accurately selecting the optimal number and configuration of P/D instances after scaling to avoid GPU idleness or overload, in addition to the engineering cost of complex schedulers and KV-cache migrations.

The method proposed in this paper addresses these gaps by forecasting near-term load and proactively resizing P-instances and D-instances according to an analytically derived optimal P/D ratio, thereby mitigating resource waste and overload caused by suboptimal P/D instance scheduling.

IV. SYSTEM MODEL

This section presents the system model of DOPD, covering the following aspects: 1) Workload characterization. 2) The optimal P/D ratio calculation. 3) Modeling of P-instance. 4) Modeling of D-instance.

A. Workload Characterization

Unlike traditional machine-learning workloads with fixed input dimensionality, LLMs workloads are substantially more heterogeneous. Each user request to an LLM may have a different input length, which in turn yields different per-request computational costs. Because mainstream LLMs are Transformer-based, the computational pressure concentrates in the attention and feed-forward components. The attention computation can be written as

$$\text{output}_{Attn} = \text{softmax}(QK^T)V, \quad (1)$$

where Q, K, V are the query, key, and value matrices produced from the input sequence by linear projections. The asymptotic complexity of the attention operation is

$$C_{attn}(ISL) = \mathcal{O}(ISL \cdot H^2 + ISL^2 \cdot H), \quad (2)$$

where ISL denotes the input-sequence length and H denotes the model hidden size. The feed-forward computation can be abstracted as

$$\text{Output}_{FFN} = \text{Linear}(\text{Linear}(\text{Linear}(\text{output}_{Attn}))) \quad (3)$$

whose complexity is approximately

$$C_{ffn}(ISL) = \mathcal{O}(ISL \cdot H \cdot H'), \quad (4)$$

where H' denotes the intermediate size of the feed-forward layer (typically $H' \geq H$). Thus the per-request computational cost can be expressed as

$$C(ISL) = C_{attn}(ISL) + C_{ffn}(ISL). \quad (5)$$

To reason about heterogeneous requests we lift this per-request cost to the level of the input-length distribution f_{ISL} and consider moments of ISL . In particular the expected per-request cost is

$$\begin{aligned} \mathbb{E}[C] &= \int C(x) f_{ISL}(x) dx \\ &= \kappa_1 H^2 \mathbb{E}[ISL] + \kappa_2 H \mathbb{E}[ISL^2] + \kappa_3 H H' \mathbb{E}[ISL], \end{aligned} \quad (6)$$

where constants $\kappa_1, \kappa_2, \kappa_3$ hide implementation-level factors. Note that

$$\mathbb{E}[ISL^2] = \text{Var}(ISL) + \mathbb{E}[ISL]^2, \quad (7)$$

and because of the ISL^2 term in Eq. (2), the cost function $C(ISL)$ is convex in ISL , so by Jensen's inequality we have

$$\mathbb{E}[C] \geq C(\mathbb{E}[ISL]), \quad (8)$$

which quantifies how heterogeneity (and in particular variance) amplifies average computation beyond what a mean-length estimate would predict.

Empirically, inference workloads commonly exhibit a long-tail distribution: a small fraction of extremely long requests requires the service to retain the capability to handle such tails. A standard heavy-tail model is the Pareto law

$$\Pr\{ISL > x\} = \left(\frac{x_m}{x}\right)^\alpha, \quad \text{s.t. } x \geq x_m, \alpha > 0, \quad (9)$$

where the tail index α controls the existence of moments (for example, the variance is finite only if $\alpha > 2$). When α is small the second moment in (Eq. (7)) can be very large (or formally divergent), explaining why a tiny fraction of requests can dominate overall compute and memory pressure.

The high variance in input length makes aggregating prefill and decoding requests problematic. Because the per-step inference time of the two request types can differ dramatically, batching them together causes severe mutual interference and substantially degrades system performance. This effect can be formalized through queueing approximations. If requests arrive with (time-varying) rate $\lambda(t)$ and service time S satisfies $\mathbb{E}[S] \propto \mathbb{E}[C]/\text{COMPUTE}_{\text{speed}}$, then Little's law $L = \lambda W$ links occupancy L and mean sojourn W , and Kingman's heavy-traffic approximation for a $G/G/1$ queue gives the mean waiting time

$$W_q \approx \frac{\rho}{1-\rho} \cdot \frac{c_a^2 + c_s^2}{2} \mathbb{E}[S], \quad (10)$$

where $\rho = \lambda \mathbb{E}[S]$ is load, c_a^2 is the squared coefficient of variation of inter-arrival times and $c_s^2 = \text{Var}(S)/\mathbb{E}[S]^2$ is that of service time. Because c_s^2 grows with $\text{Var}(ISL)$ via (Eq. (5)) and (Eq. (7)), mixing requests with very different ISL (or mixing prefill and decoding) inflates c_s^2 , increasing W_q and thus end-to-end latency.

The complexity of LLM inference service workloads extends further. Requests arrive in short-lived bursts and the instantaneous concurrency seen by the service varies over time. Such burstiness can be modeled by Markov-Modulated Poisson Processes (MMPP) or compound-Poisson models, which capture non-stationary and over-dispersed arrivals (i.e., $c_a^2 > 1$). The peak concurrency in the next service epoch may be orders of magnitude larger (or smaller) than in the previous epoch. Consequently, adaptive resource provisioning that accounts for both the distribution of request lengths (via moments such as $\mathbb{E}[ISL]$, $\text{Var}(ISL)$ and tail index α) and rapidly changing concurrency (via time-varying $\lambda(t)$ or MMPP parameters) is essential for maximizing resource utilization. This nonstationary and bursty nature can cause serious resource waste in PD-Disaggregation systems because a fixed P/D ratio is suitable only for a restricted class of workloads.

To address these challenges, DOPD periodically feeds background-collected telemetry into an ARIMA-based [33] load predictor and issues regular forecasts of the future average request length and concurrency. These forecasts are combined with the moment-based cost estimates in Eq. (6) and the queueing-delay estimates such as Eq. (10) to drive DOPD's dynamic P/D ratio computation and elastic resizing of P-instances and D-instances, enabling the system to pre-allocate resources commensurate with the anticipated heterogeneous and time-varying workload.

B. The Optimal P/D Ratio Calculation

1) *The Object of this Optimal P/D Ratio:* When all requests are served via remote prefill (perform prefill in P-instance), the prefill-to-decoding workflow naturally forms a producer-consumer pair. P-instances produce prefill-completed requests (together with KV-cache), and D-instances consume those prefill-completed requests to perform token generation. Therefore, balancing production and consumption is essential to reduce resource waste. And system throughput for disaggregated inference is largely determined by the concurrency (the number of in-flight requests in system) that each D-instance can sustain, because each generated token must be produced by a D-instance and returned to the frontend. The maximum concurrency a D-instance can support depends on request length as well as on GPU memory capacity and memory bandwidth. Therefore, the optimal P/D ratio should (i) maximize the aggregate concurrency supported by D-instances and (ii) select a corresponding number of P-instances so that neither P-instances nor D-instances remain idle for appreciable periods.

2) *Method for Computing the Optimal P/D Ratio:* To simplify the following calculations, assume all incoming requests have the same input sequence length ISL and output sequence length OSL . First, based on GPU memory bandwidth, GPU memory capacity M_{gpu} , model size M_{model} , and the CUDA graph inference configuration in use, determine a suitable parallelization configuration (e.g., tensor parallelism). Note that the maximum parallelism of a D-instance must be bounded by both memory capacity and bandwidth constraints. The true limit is the minimum of the two. From the memory-capacity perspective, for tensor parallel size TP , the remaining memory available for KV-cache on a D-instance is

$$V_{mem} = (M_{gpu} - M') \times TP - M_{model} \quad (11)$$

where M' encompasses peak activation-parameter memory (which varies with the model's maximum sequence length) and other ancillary GPU memory usage. From the bandwidth perspective, since KV-cache is stored separately on each GPU under tensor parallelism and is continuously read during decoding, we estimate the maximum KV-cache transferable in a single decoding based on the SLO decoding time t_d^{SLO} , GPU bandwidth BW , tensor parallel size TP , and an achievable bandwidth utilization factor α (empirically, $\alpha = 0.6$ is considered excellent). Thus, the maximum amount of KV-cache that can be transferred within a single decoding-step SLO-constrained interval t_d^{SLO} is approximately

$$V_{BW} = t_d^{SLO} \times \alpha \times TP \times BW \quad (12)$$

Next, given the per-token memory footprint M_{token} for the model, the D-instance concurrency cc_d under the average sequence lengths is:

$$cc_d = \frac{\min(V_{mem}, V_{BW})}{(ISL + OSL/2) \times M_{token}} \quad (13)$$

Additionally, the inference engine's maximum CUDA graph batch capacity cc_g further constrains per-step batch size. Hence the effective decoding concurrency is

$$cc_d = \min(cc_d, cc_g) \quad (14)$$

In practice, to improve headroom for bursty traffic one may choose TP so that an instance can support up to $0.9 \times cc_g$ concurrency. After obtaining the D-instance's suitable TP and maximum concurrency, we calculate the required production capacity of a single P-instance. Since the prefill stage often becomes the compute bottleneck, some systems set the P-instance batch size as low as 1. In such case, each P-instance produces one request per prefill execution. In an autoregressive model, one prefill inference is performed per request, followed by multiple decoding inferences. Hence, while a D-instance is decoding one request, a P-instance may produce multiple prefill-completed requests. The D-instance then accumulates these into batches for decoding. With fixed request lengths, the maximum number of prefill runs per P-instance during a single D-request decoding equals the batch size needed to saturate the D-instance. When n_p P-instances and n_d D-instances all reach their maximum concurrency without idle or overload, the system achieves maximum throughput with balanced production and consumption. The optimal P/D ratio satisfies:

$$n_p \times \left(\frac{1}{t_p}\right) = n_d \times \frac{cc_d}{(t_d \times OSL)} \quad (15)$$

where t_p represents the time for P-instance to execute a single sequence, and t_d represents the time for D-Instance to execute a single batch single step. Thus, we derive an analytical formula for the optimal P/D ratio.

Applying this method yields a deployment configuration that, for a given load, selects the resource allocation between P-instances and D-instances so that both roles exhibit near-zero idle time during steady-state inference and the overall system throughput is maximized. The proposed DOPD system employs an ARIMA-based predictor to forecast near-term workload characteristics from historical telemetry, including the future average ISL , the future average OSL , and the expected average concurrency. DOPD maps these forecasts to profiled Prefill and Decode performance metrics, computes the optimal P/D ratio and the corresponding instance configurations, and then enacts non-disruptive instance adjustments. The detailed calculation and execution steps are described in subsection V-D and Algorithm 2.

C. Modeling of P-instance

For P-Instances, an excessively large TP (tensor parallel size) can be detrimental. Prefill requests are compute-bound, which imposes high demands on GPU compute capability. Consequently, many modern systems configure P-instances conservatively with very small prefill batch sizes (sometimes batch size 1). When prefill batch sizes are small, the communication latency introduced by tensor parallelism distributed inference can dominate the prefill execution time. Communication overhead therefore becomes a significant cost that reduces the acceleration gains from tensor parallelism. To model this trade-off briefly, let $C(ISL)$ denote the compute work for a prefill request of input length ISL . We formulate the prefill latency under a given TP as the sum of an ideally accelerated compute term and a communication term:

$$T_{prefill}(ISL, TP) = \frac{C(ISL)}{S(TP)} + \tau(TP), \quad (16)$$

Algorithm 1 Prefill Requests Scheduler**Variables:**

i_{next} Length threshold for immediate processing
 $timeout$ Requests maximum waiting time
 PREFILL_QUEUE Remote prefill requests queue
 TIMER Record request wait time
 REQS_BATCH Collection of requests to be batched

Require: i_{next} , PREFILL_QUEUE, TIMER, REQS_BATCH

```

1: initialize TIMER, REQS_BATCH
2: loop
3:   Get reasonable  $timeout$  based current batch
4:   if REQS_BATCH.ALL_LENGTH()  $\geq i_{next}$ 
   or (TIMER.DURATION()  $\geq timeout$  and
   len(REQS_BATCH) > 0) then
5:     Inference and reset REQS_BATCH
6:     TIMER.CLEAR()
7:   end if
8:    $req \leftarrow$  PREFILL_QUEUE.POP()
9:    $\triangleright$  PREFILL_QUEUE.POP() returns null if empty
10:  if  $req = \text{null}$  then
11:    if len(REQS_BATCH) > 0 then
12:      Inference and reset REQS_BATCH
13:      TIMER.CLEAR()
14:    else
15:      continue
16:    end if
17:  end if
18:  if  $req.length < i_{next}$  then
19:    REQS_BATCH.ADD( $req$ )
20:    if len(REQS_BATCH) = 1 then
21:      TIMER.START()
22:    end if
23:  else
24:    Inference  $req$ 
25:  end if
26: end loop

```

where $S(TP)$ is the effective speedup (with $S(TP) \leq TP$ and typically showing diminishing returns) and $\tau(TP)$ models tensor parallelism-induced communication overhead (which is non-decreasing in TP). Eq. (16) explains why, for small batch sizes or small models, increasing TP can increase $T_{prefill}$ when $\tau(TP)$ dominates the compute acceleration.

Therefore, TP is often set to just the right value to support the maximum model sequence length for inference requests. If a single-instance load becomes excessive, one can address it by scaling out (adding identical P-instances).

From subsection IV-B, the calculation of the optimal P/D ratio depends on the input and output lengths of requests in the workload. Consequently, under a high-concurrency mixed-length workload, a system configuration obtained from the average input and output lengths may become mismatched as lengths vary. To address this, short requests in the pending workload can be batched up to the input length corresponding to the system configuration so that the system adapts to the current load. To avoid degrading SLO attainment due to such

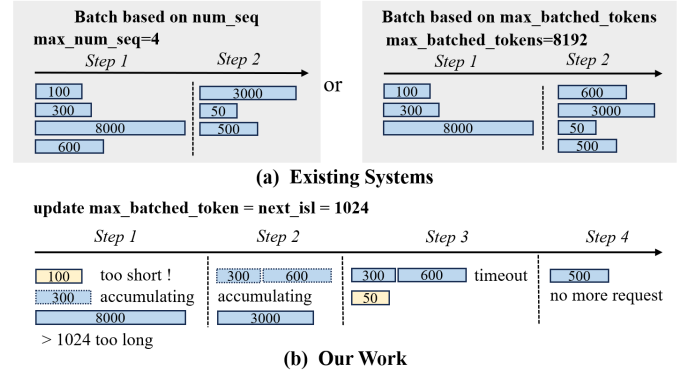


Figure 4: Comparison of prefill request scheduling solutions. All blocks represent the prefill inference process for sequences, and where the blue block represents the prefill inference for that sequence performed in a P-instance, and the yellow block represents the prefill inference performed in a D-instance. The solid block represents processing, and the dashed block represents unprocessed at the current step and still pending processing.

batching, we should first model and analyze request queuing and timeout selection. To reason about queuing delay and timeout selection formally, let incoming requests follow an average arrival rate λ , and denote the mean prefill service time by $\mathbb{E}[S]$ (where $\mathbb{E}[S] = \mathbb{E}[T_{prefill}]$ given the chosen TP and batching strategy). Then the system utilization is

$$\rho = \lambda \mathbb{E}[S]. \quad (17)$$

By Little's law the average number of requests in system L and the mean sojourn time W satisfy $L = \lambda W$. For non-exponential arrival/service statistics, the (Kingman) heavy-traffic approximation gives the queueing waiting time W_q same as Eq. (10), where c_a^2 and c_s^2 are the squared coefficients of variation of inter-arrival and service times respectively. Eq. (10) and Eq. (16) allow us to (i) evaluate how a choice of TP affects $\mathbb{E}[S]$ and hence ρ , and (ii) set the maximum waiting timeout $T_{timeout}$ to control the contribution of W_q to TTFT. For example, a conservative choice is to enforce

$$T_{timeout} \geq \alpha \cdot W_q \quad (18)$$

for a safety factor $\alpha \in (0, 1]$ to bound expected extra waiting.

Because LLM request lengths vary widely, the conventional first-come-first-served batching policy—taking the first n queued requests and forming a batch—can be suboptimal (as shown in Figure 4(a)). Such a policy may batch long and short requests together, causing long requests to push the GPU into a compute bottleneck and mismatch of system instances resource configuration, resulting in uneven resource utilization. This can be mitigated by a length-aware internal scheduling policy. When a P-instance dequeues requests from the prefill queue, it inspects each request's input length and applies the following logic.

If a request's length exceeds a predefined threshold, the P-instance dispatches it immediately for inference (as shown in step 1 and step 2 in the flow of Figure 4(b)). In DOPD, we set this threshold to the ARIMA-based predictor's one-step

forecast of the next average input sequence length (denoted $next_isl$ in Figure 4(b)),

$$i_{next} = \widehat{ISL}_{t+1|t}, \quad (19)$$

so that naturally long requests are not delayed by batching short ones. If a request is short, the instance accumulates short requests until either an accumulated-length constraint or a waiting-time constraint is met (as shown in step 1 and step 2 in Figure 4(b)). The batching-selection can be formalized as a (0-1) knapsack problem: given a set of candidate short requests indexed by i with input lengths w_i and benefit values v_i (e.g., estimated throughput improvement or reduced per-request overhead), choose binary indicators $x_i \in \{0, 1\}$ to

$$\begin{aligned} \max_{\{x_i\}} \quad & \sum_i v_i x_i \\ \text{s.t.} \quad & \sum_i w_i x_i \leq W_{batch}, \\ & x_i \in \{0, 1\}, \end{aligned} \quad (20)$$

where W_{batch} is the accumulated-length threshold (an operational counterpart in Algorithm 1 i_{next}). In online settings we recommend a greedy heuristic that orders candidates by v_i/w_i (value per token) to maintain low scheduling overhead.

To avoid excessive waiting for short requests, a maximum waiting time is enforced. Once accumulated requests have waited longer than this timeout, the batch is executed immediately (as shown in step 3 in Figure 4(b)). Combining the above models—TP speedup/communication trade-off (Eq. (16)), queuing delay estimates ((10)), and knapsack-style batching selection (Eq. (20))—yields a principled length-aware prefill scheduler that (i) selects TP to minimize expected $E[T_{prefill}]$ under realistic $\tau(TP)$, (ii) sets $T_{timeout}$ as a function of W_q to bound TTFT contribution from queuing, and (iii) forms batches to maximize utilization while limiting per-request added waiting. Algorithm 1 implements this scheduling process in practice. It can be observed that the scheduling routine incurs very low overhead. Its dominant cost lies in queue maintenance, so the time complexity per dequeue operation is $\mathcal{O}(N)$, where N denotes the number of requests in the queue.

D. Modeling of D-instance

The decoding phase is primarily constrained by memory rather than compute. Therefore, D-instances typically process multiple requests concurrently using batching to improve device utilization and system throughput. For LLM inference services, the D-instance batch size directly determines aggregate throughput: larger batch sizes generally yield higher throughput. The maximum feasible batch size for a D-instance is mainly determined by the GPU memory available for storing the KV-cache. Consequently, the distributed deployment parallelism for D-instances must be chosen carefully.

A prevalent strategy is to deploy D-instances using tensor parallelism because with TP way tensor parallelism each GPU holds only $\frac{1}{TP}$ of the model weights, substantially reducing per-GPU memory footprint. This configuration both frees GPU memory for larger KV-cache and distributes computation

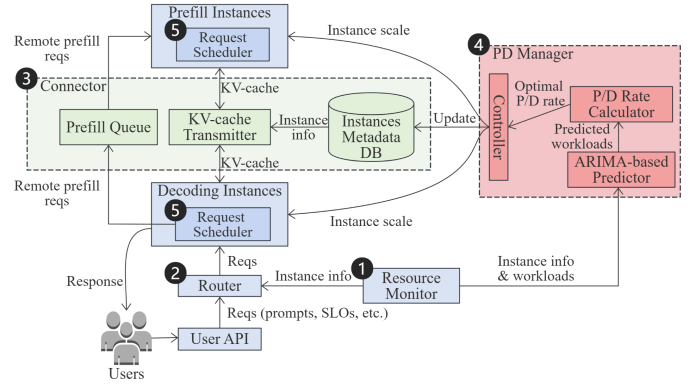


Figure 5: DOPD system architecture.

across GPUs. When batch sizes are large, the relative communication overhead of tensor parallelism is small, making tensor parallelism deployment particularly suitable for D-instances. In general, increasing TP allows a D-instance to support a larger maximum batch size and thus improves the system’s ability to handle high-concurrency workloads. However, setting TP excessively large may lead to resource waste. Guidelines for selecting an appropriate TP for D-instances are provided in subsection IV-B.

V. SYSTEM DESIGN AND IMPLEMENTATION

We propose a method to accurately compute an appropriate P/D ratio based on current load and to dynamically reconfigure the P-instances and D-instances accordingly, so as to improve throughput with minimal GPU resources and meet the SLOs attainment, thereby achieving higher effective throughput in PD-Disaggregation LLM inference systems. Building on these objectives, we extend the Dynamo framework to realize a dynamically optimal PD-Disaggregation inference system. The system comprises five principal components: (1) Resource Monitor, (2) Router, (3) Connector, (4) PD Manager, and (5) Request Scheduler.

A. Resource Monitor

The Resource Monitor (denoted by ① in Figure 5) is a core subsystem responsible for collecting cluster- and instance-level performance metrics and load indicators to construct profiles for short-term load prediction and scheduling decisions. Both the Request Scheduler and the PD Manager rely on the Resource Monitor for up-to-date telemetry. Monitored signals include the number of P-instances, available GPU memory on D-instances, KV-cache utilization on D-instances, the size of the prefill queue, and so on. The Resource Monitor also records recent averages of TTFT, TPOT, ISL, and OSL with Prometheus [34] to meet the SLOs attainment and to provide inputs used by the PD Manager and the Request Scheduler.

B. Router

The Router (denoted by ②) aggregates KV-cache information across all D-instances and routes incoming user requests to the most suitable instance. The Router is integrated with

prefix-caching logic. For each request it computes the expected KV-cache hits on each D-instance, combines that information with per-instance load reported by the Resource Monitor, and preferentially forwards the request to the instance with the highest expected cache-hit count and the lowest inferred load. Concretely, upon request arrival the server forwards the request to the Router, which queries the Resource Monitor for current per-instance loads, retrieves KV-cache metadata for each D-instance, computes a prefix cache-hit ratio per instance, evaluates an inference-cost metric that incorporates both cache locality and instance load, and dispatches the request to the D-instance with the minimum inferred cost.

C. Connector

The Connector (denoted by ③) provides inter-instance connectivity, maintains the queue of requests awaiting remote prefill, and implements end-to-end KV-cache transfers between P-instances and D-instances. The Connector contains three primary components: (1) an instances metadata DB, (2) a prefill queue, and (3) a KV-cache transmitter.

The instances metadata DB is implemented as an etcd service that registers the IDs of all P-instances and D-instances together with the addresses of their KV-cache blocks whenever a new instance joins the cluster. Assignment of each remote prefill request to corresponding P-instances and D-instances is derived from this registry.

The prefill queue is implemented using a NATS service acting as a first-in-first-out (FIFO) queue that holds requests awaiting remote prefill (prefill inference in P-instance). Whenever a request is slated for remote prefill it is enqueued in the prefill queue. P-instances continuously poll this queue and dequeue requests into their local processing queues.

The KV-cache transmitter leverages NVIDIA's open-source NIXL [22] communication library to perform high-performance GPU-to-GPU transfers of KV-cache blocks, thereby eliminating KV-cache transfer latency as a dominant bottleneck in PD-Disaggregation.

D. PD Manager

The PD Manager (denoted by ④) is a component that can calculate the optimal P/D ratio based on historical load and adjust the instances in the system to this ratio. As argued above in Section IV, the P/D ratio is a decisive factor for performance in PD-Disaggregation LLM inference systems. Accurately computing an optimal P/D ratio requires accounting for multiple low-level characteristics, for example, GPU memory capacity, GPU memory bandwidth and other factors.

As argued above in subsection IV-B, the optimal P/D ratio is determined by request input and output lengths. In real-world deployments, however, inference load varies over time and thus the optimal P/D ratio shifts accordingly. Hence it is necessary to adjust the P/D ratio dynamically in response to load fluctuations. Prior to service deployment we profile the target model and GPU to obtain, across multiple tensor parallelism configurations and for varying sequence lengths and concurrency levels, TTFT, TPOT, and other relevant metrics for both prefill and decoding phases. We first profile a single P-instance

Algorithm 2 Dynamic P/D Ratio Adjustment

Variables:

CC_{max} The D-instance's concurrency cap
 $ttft[\cdot]$ TTFT profiling table
 $tpot[\cdot][\cdot]$ TPOT profiling table
 PRED ARIMA predictor
 INTERP Interpolator instances
 T Monitoring interval
 t_{last}, t_{cur} Last record and current timestamps
 i_{last}, i_{next} Last and predicted input size
 o_{last}, o_{next} Last and predicted output size
 r_{last}, r_{next} Last and predicted request count
 TP_p Best tensor parallel size of P-instance
 TP_d Best tensor parallel size of D-instance
 $ttft_{next}, tpot_{next}$ Interpolated performance metrics
 R_{opt} Optimal P/D (prefill/decoding) ratio
 n_p, n_d Next number of P-instance and D-instance
 ADJUST_PD Instance adjustment action

Require: $TP_p, TP_d, CC_{max}, T, ttft[\cdot], tpot[\cdot][\cdot]$

- 1: Initialize PRED, INTERP, t_{last}
- 2: **loop**
- 3: $t_{cur} \leftarrow \text{TIME}$
- 4: **if** $t_{cur} - t_{last} > T$ **then**
- 5: $i_{last}, o_{last}, r_{last} \leftarrow \text{RESOURCEMONITOR}$
- 6: $t_{last} \leftarrow t_{cur}$
- 7: PRED.ADD_DATA_POINT($i_{last}, o_{last}, r_{last}$)
- 8: ARIMA one-step forecast (where $p, q, \mu, \varphi, \theta, \hat{\epsilon}$ denote ARIMA parameters and estimated residuals):

$$\hat{X}_{t+1|t} = \mu + \sum_{j=1}^p \varphi_j X_{t+1-j} + \sum_{k=1}^q \theta_k \hat{\epsilon}_{t+1-k}$$

- 9: $i_{next} = \hat{I}_{t+1|t}, o_{next} = \hat{O}_{t+1|t}, r_{next} = \hat{R}_{t+1|t}$
 - 10: $ttft_{next} \leftarrow \text{INTERP}(ttft[\cdot], i_{next})$
 - 11: $tpot_{next} \leftarrow \text{INTERP}(tpot[\cdot][\cdot], r_{next}, \frac{i_{next} + o_{next}}{2})$
 - 12: $R_{opt} \leftarrow \frac{r_{next}}{(o_{next} \times tpot_{next}) / ttft_{next}}$
 - 13: $n_d \leftarrow \lceil r_{next} / CC_{max} \rceil$
 - 14: $n_p \leftarrow R_{opt} \times n_d$
 - 15: ADJUST_PD(n_p, TP_p, n_d, TP_d)
 - 16: **end if**
 - 17: **end loop**
-

across a range of input sequence lengths to obtain accurate TTFT measurements as a function of input length. Similarly, we profile a single D-instance across combinations of sequence lengths and batch sizes to obtain precise TPOT measurements as a function of sequence length and batch size. These per-instance profiles substantially improve the fidelity of the P/D ratio computation. These profiles guide parallel-configuration choices during scaling and provide expected TTFT/TPOT values for given sequence lengths and concurrency. "Initialize INTERP" in Algorithm 2 performs this process.

At runtime, the Resource Monitor maintains a recent distribution of request lengths. To avoid the overhead of expensive predictions at scale, we employ a lightweight time-series model (ARIMA) to forecast the future average input and

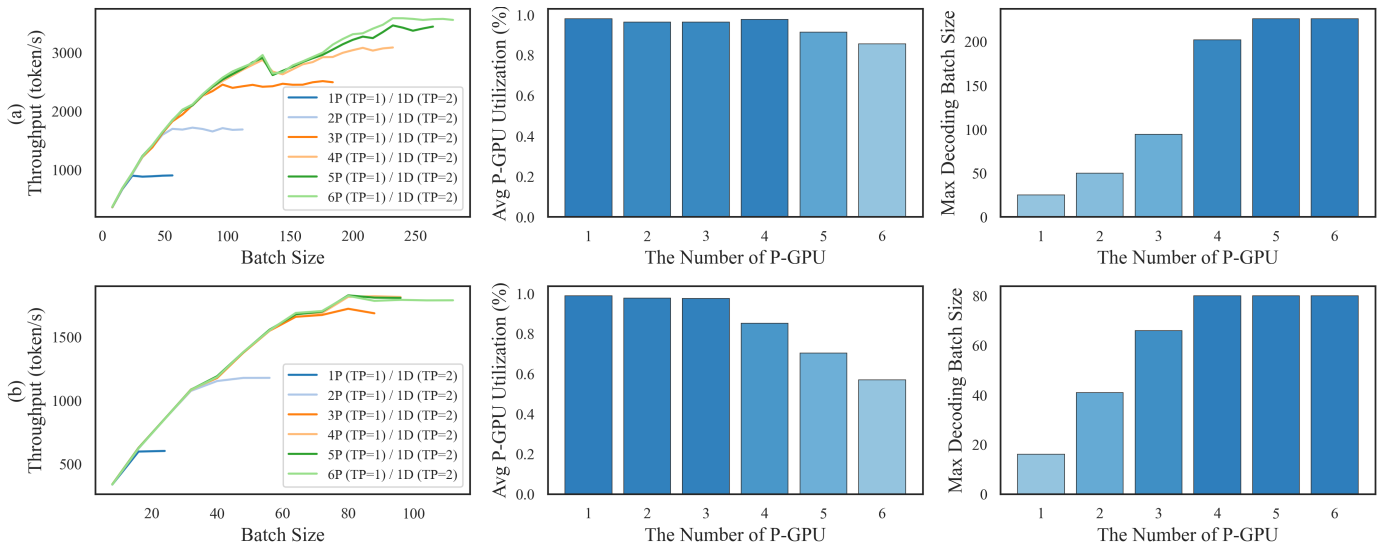


Figure 6: Optimal P/D ratio validation experiment results for varying numbers of P-instances and a single D-instance with $TP = 2$ under (a) fixed input/output lengths of 1000/150. The computed optimal number of P-instances for 1000/150 is approximately 4.58. (b) fixed input/output lengths of 3000/300. The precomputed optimal number of P-instances for 3000/300 is approximately 3.18.

output lengths. We map these forecasts to profiled TTFT/TPOT values and compare them with the recently observed averages from the Resource Monitor to derive correction factors. To reduce forecast error, we combine the derived correction factors with the forecasted average sequence lengths and the profiled performance parameters to compute the projected optimal P/D ratio.

After obtaining an accurate optimal P/D ratio, we replace Dynamo’s original SLA-based (Service-Level Agreement) and load-based scheduling policies with the optimal P/D ratio-based scheduling strategy while preserving Dynamo’s ability to dynamically reconfigure instance characteristics. DOPD first jointly considers the factors listed above to determine the optimal tensor parallel size TP for P-instances and D-instances, and then performs instance adjustments according to the computed optimal P/D ratio. This design enables accurate forecasting of a future, workload-appropriate P/D ratio from historical telemetry and supports non-disruptive (zero-downtime) elastic resizing of P-instances and D-instances to promptly accommodate time-varying user request loads.

Algorithm 2 summarizes the procedure for forecasting future load, deriving the optimal P/D ratio, and executing instance adjustments. The dominant cost in this pipeline arises from the ARIMA predictor used for load forecasting. After each prediction we compare the forecast to subsequently observed telemetry. If the prediction error is large we re-fit the ARIMA parameters, otherwise we retain the current model. When refitting is required, the ARIMA update cost is $\mathcal{O}(N \cdot (p+q)^2)$, where N is the number of historical records used (typically treated as a fixed constant) and p, q are the ARIMA orders. If no refit is needed, the prediction cost is only $\mathcal{O}(p+q)$. Therefore the worst-case time complexity of the forecasting component is $\mathcal{O}(N \cdot (p+q)^2)$. All remaining operations (table lookups, arithmetic, and control decisions) are low-cost. In practice, the scheduling and forecasting latency remains small (well under 1s in our tests), while system recon-

figuration intervals are typically on the order of hundreds of seconds. Therefore, the runtime overhead of DOPD’s dynamic scheduling is negligible relative to the adjustment timescale, demonstrating that the proposed scheduling strategy is highly efficient.

E. Request Scheduler

The Request Scheduler (denoted by ⑤) is built into P-instances and D-instances to arrange requests reasonably, allowing the PD-Disaggregation system to better cope with mixed requests. Even with an analytically derived P/D ratio for average input/output lengths, Dynamo’s original scheduling mechanism performs poorly when the request-length distribution is highly skewed. For example, an optimal ratio tuned for an average length $ISL = 1000$ may be suboptimal when the workload comprises roughly half the requests with $ISL = 100$ and half with $ISL = 1900$. To mitigate this, we group and batch requests by their input-token counts. Under high concurrency, short requests are batched according to their predicted future lengths to leverage kernel efficiency, reducing the mismatch between short-length load and the provisioned P/D ratio. Long requests, whose computational cost is inherently high, are not merged and are dispatched to P-instances for immediate execution.

Moreover, ultra-short requests often do not benefit from PD-Disaggregation because their prefill compute cost is negligible and KV-cache transfer overhead becomes significant. For these cases we employ PD-aggregation: merging their prefill on P-instances with other requests’ decoding on D-instances avoids unnecessary KV-cache transfers and relieves prefill queue pressure (illustrated by the yellow blocks in step 1 and step 3 of the flow in Figure 4(b)). Using this request-scheduling scheme, our experiments on realistic workloads demonstrate substantial improvements in maximum concurrency, throughput, and TTFT without changing the global P/D ratio. Detailed results appear in Section VI.

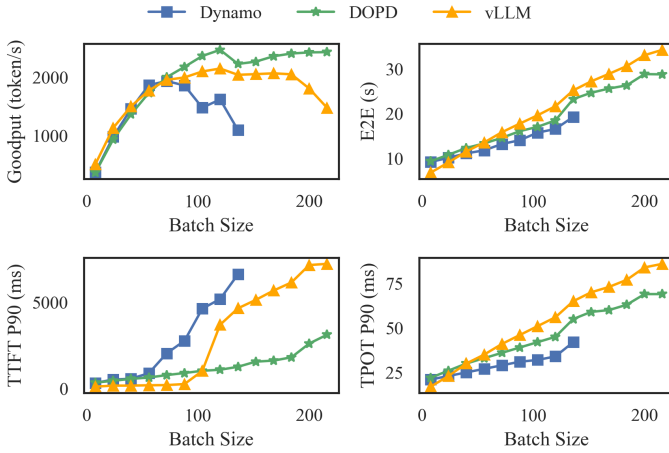


Figure 7: Static P/D ratio on real Azure workloads experimental results compared to aggregation methods.

VI. PERFORMANCE EVALUATION

This section carries out experimental evaluation of the proposed DOPD system. It discusses configuration and analyses of our experiments and results along with scalability of DOPD and the directions of future research.

A. Evaluation Setup

1) *Testbed:* We conduct experiments on a local cluster composed of 8 NVIDIA H100-SXM-80GB [12] GPUs.

2) *LLM models:* For inference-performance evaluation we select two representative models used in prior works and industries test suites: facebook/opt-30b [35] and RedHatAI/DeepSeek-R1-Distill-Llama-70B-FP8-dynamic [36] (hereafter referred to as Llama-70B-FP8). Both models are widely adopted in academic and industrial research.

3) *Datasets:* We employ two production workload traces collected from Microsoft (BurstGPT [37] and Microsoft Azure Traces [38]), and we use the ShareGPT [39] dataset for request contents. These traces originate from real production environments and thus provide realistic workload characteristics.

4) *Resource monitoring:* Real-time, continuous performance monitoring across the devices is critical. We track GPU utilization, GPU memory-bandwidth utilization, GPU memory utilization, as well as ISL, OSL, TTFT, and TPOT over sliding windows. To collect and aggregate telemetry we leverage NVIDIA’s NVML [40] for low-level GPU metrics and Prometheus [34] for metrics aggregation and retention.

B. Baselines and Metrics

1) *Baselines:* We perform two categories of experiments: static and dynamic.

a) *Static experiments:* Under a fixed P/D configuration we compare the following systems:

- **DistServe** [18]: a representative PD-Disaggregation framework with strong performance characteristics.
- **Dynamo** [32]: the most feature-complete open-source PD-Disaggregation framework.
- **vLLM** [24]: a state-of-the-art open-source LLM inference system with broad adoption.

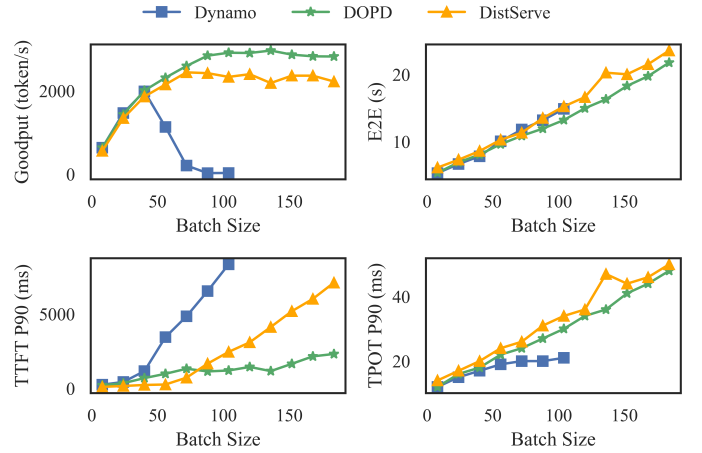


Figure 8: Static P/D ratio on real Azure workloads Experimental results compared to disaggregation methods.

b) *Dynamic experiments.:* Because mature dynamic PD-Disaggregation scheduling is not widely available outside Dynamo, we compare DOPD against two Dynamo scheduling policies:

- **DYN-LOAD:** a load-based scheduler that scales based on runtime utilization thresholds.
- **DYN-SLA:** an SLA-aware scheduler that derives scaling decisions from real-time inference monitor metrics.

Both Dynamo policies consider multiple runtime signals and perform real-time scheduling.

2) *Metrics:* We evaluate using four widely adopted metrics:

- **TTFT:** elapsed time from request issuance until the first output token is produced.
- **TPOT:** average interval between successive tokens after the first, which reflects token-generation pacing.
- **Goodput:** the rate of useful tokens successfully delivered per unit time under SLO constraints (TTFT < 2s and TPOT < 0.08s), which measures effective, SLO-attainment throughput.
- **Throughput:** the total number of tokens generated per second irrespective of latency or SLO attainment, which indicates raw processing capacity.

3) *Validation of the Optimal P/D Ratio:* We first deploy Dynamo with the Llama-70B-FP8 model, varying the number of P-instances (each on 1 H100 GPU) while fixing the number of D-instances to one (with $TP = 2$ across 2 H100 GPUs). Prior to service launch, our computation yields an optimal P/D ratio of approximately 4.58, with the D-instance supporting a maximum concurrency of about 235, indicating that roughly 4.58 P-instances suffice to balance production and consumption.

During each experiment we issue inference requests with fixed input length $ISL = 1000$ and output length $OSL = 150$ at varying concurrency levels (concurrency is defined as the number of in-flight requests in system). Figure 6(a) illustrates throughput under the fixed 1000/150 workload. It shows a near-linear increase in maximum throughput as the number of P-instances increases from 1 to 4. Beyond 4, throughput growth from 4 to 5 slows markedly, and from 5 to 6 is

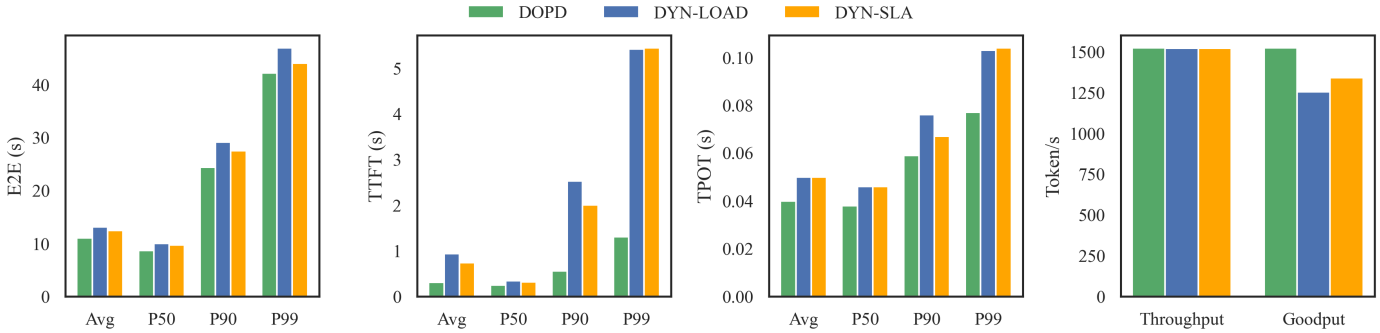


Figure 9: Dynamic scheduling experimental results under real-world BurstGPT workloads. "DYN-LOAD" represents the dynamic scheduling strategy experiment based on load. "DYN-SLA" represents the dynamic scheduling strategy experiment based on SLA.

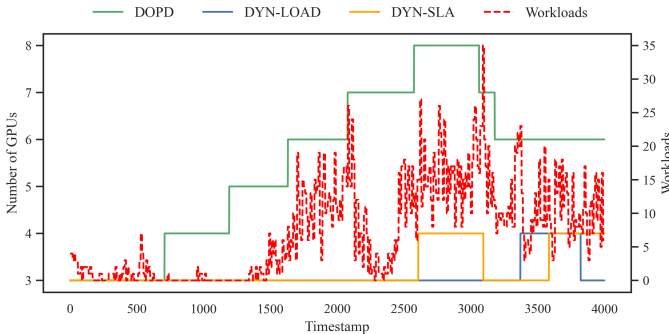


Figure 10: Variation of provisioned GPU count and inference workload over time in the dynamic-scheduling experiment. Solid lines show the number of GPUs provisioned by each scheduling strategy (DOPD, DYN-LOAD and DYN-SLA). These correspond to the left vertical axis. The dashed line shows the instantaneous inference workloads (request rate) and corresponds to the right vertical axis.

negligible. Concurrently, the average GPU utilization of P-instances (as shown in Figure 6(a)) indicates idle GPU time only when the number of P-instances exceeds 4. Moreover, the D-instance's maximum batch size (Figure 6(a), right) plateaus at 80 for P-instances > 4 , confirming no gain from additional P-instances. These observations validate our computed optimal P/D ratio.

We further compute that for input/output lengths of 3000/300, the D-instance supports a maximum concurrency of approximately 78 (Due to experimental resource constraints, we can only configure D-instance like this), yielding an optimal P-instance count of about 3.18. Repeating the experiment under the 3000/300 workload produces analogous results, further confirming the accuracy of our calculation method.

4) Comparison of Static P/D Inference-Performance: We extract the first 1024 entries from Microsoft Azure traces and use ShareGPT as the source of request content, generate a request set with average input/output lengths of approximately 1024/245. We then show two sets of experiments.

First, we compare DOPD with a representative PD-aggregation system and a PD-Disaggregation baseline using the Llama-70B-FP8 model. The aggregation baseline (vLLM) is deployed on 4 H100 GPUs, whereas both disaggregation baselines (Dynamo and DOPD) are configured as 2P (TP=1) / 2D (TP=2). We generate inference workload

from the Microsoft Azure traces and replay it to each deployment. Results are reported in Figure 7, which shows goodput, TTFT, TPOT, and end-to-end latency under the same workload. Compared to PD-aggregation (i.e., vLLM), DOPD reduces P90 TPOT from 0.097s up to 0.079s and increases goodput by up to 1.5 \times . Under reasonable SLO constraints (violation rate $< 5\%$), DOPD also supports a substantially higher maximum concurrency, rising from 72 to 112.

Second, we evaluate three PD-Disaggregation systems using the facebook/opt-30b model. In these experiments each system uses 1 H100 GPU as the P-instance and 4 H100 GPUs as D-instances ($TP = 4$). Results appear in Figure 8. As concurrency increases, DOPD's benefits become pronounced: relative to a representative disaggregation system (DistServe), DOPD reduces P90 TTFT from 7.10s to 2.31s and improves goodput by up to 27%. Under the SLO constraints (violation rate $< 5\%$), the maximum supported concurrency increases from 88 to 104. Similarly, compared with Dynamo, DOPD achieves substantial improvements across all reported metrics.

5) Dynamic P/D Instance-Scheduling Performance Comparison: DOPD significantly outperforms Dynamo's built-in load-based and SLA-aware scheduling strategies under complex and highly variable inference workloads. We combine the workload of the BurstGPT dataset with the request content of the ShareGPT dataset to generate a simulated LLM inference workload. According to the timestamps in the BurstGPT trace, we replay requests to three service deployments. Here, DYN-LOAD and DYN-SLA denote Dynamo systems with dynamic scaling enabled using the load-based and SLA-aware schedulers, respectively. All three systems (DOPD, DYN-LOAD, DYN-SLA) are initially configured with one P-instance ($TP = 1$) and one D-instance ($TP = 2$) running the Llama-70B-FP8 model. Figure 10 shows the number of requests versus time (sampled every 0.1s), while the other curves plot the total number of GPUs provisioned over time under each scheduling strategy. Although DYN-SLA and DYN-LOAD adjust resource allocation in response to load changes, their scaling amplitudes and timeliness are insufficient. In contrast, DOPD's GPU count closely tracks the RPS curve. It scales out rapidly during traffic spikes and scales in promptly when load subsides. Figure 9 presents the results. From the four plots it is clear that DOPD's end-to-end latency, TTFT, TPOT, and goodput all outperform the

other baselines. As a result, DOPD achieves excellent SLOs attainment (99.4%), whereas DYN-SLA and DYN-LOAD incur worse SLO attainment (87.3% and 80.8% respectively). These results demonstrate that DOPD can promptly and judiciously scale P-instances and D-instances in response to sudden load fluctuations, substantially increasing the SLO attainment.

Discussion. DOPD’s architecture introduces a dynamic, efficient approach to PD-Disaggregation and demonstrates substantial improvements in goodput and latency under variable workloads. A key advantage of the design is its scalability. The system adjusts the P-instances and D-instances based on real-time load forecasts and the analytically derived optimal P/D ratio. This design ensures that independently scaling P-instances or D-instances does not inherently create imbalance, since the PD Manager proactively recomputes the ratio to maintain producer–consumer equilibrium. Moreover, because the scheduling algorithms incur very low overhead and the system achieves strong decoupling between instances, DOPD can intelligently and efficiently adjust instance allocations even in very large-scale cluster environments.

Despite DOPD’s robustness on realistic production traces, occasional ultra-long prompts can transiently degrade overall system performance. Such ultra-long requests are rare and therefore difficult for the predictor to anticipate. Scheduling decisions that rely on average-length signals may perform poorly when extremely long contexts suddenly appear. Future work can explore targeted mitigations for ultra-long-context interference and investigate integrations with sparse-attention mechanisms or speculative-decoding architectures to enhance generality and tail robustness. Nevertheless, DOPD provides a principled foundation for dynamic resource management in disaggregated LLM inference, striking a balance between scalability and operational practicality.

VII. CONCLUSIONS

In this paper, we proposed DOPD, a dynamic framework that combines PD-Disaggregation with dynamic adjustment of instances to improve goodput, reduce inference latency, achieve more stringent SLOs, and conserve GPU resources. We introduce a method for calculating the optimal P/D ratio and a complementary request scheduling strategy that enhances the adaptation of disaggregated systems to mixed-length workloads. The proposed P/D ratio calculation together with workload-aware scheduling enables DOPD to achieve excellent performance under complex, time-varying workloads. Through extensive experiments on realistic production traces and representative LLMs, we demonstrate that DOPD achieves up to $1.5\times$ improvement in goodput while simultaneously reducing inference latency. DOPD also achieves a near-zero SLO violation rate under real-world workloads and reliably detects load fluctuations to trigger timely elastic scaling. Our results indicate that DOPD substantially improves the inference efficiency of PD-Disaggregation architectures for LLMs, thereby facilitating their deployment in industrial environments with demanding availability and performance requirements.

REFERENCES

- [1] A. Vaswani, N. Shazeer, N. Parmar *et al.*, “Attention is all you need,” in *Proceedings of the 31st International Conference on Neural Information Processing Systems*. NY, USA: Curran Associates Inc., 2017, pp. 6000–6010.
- [2] openai. (2024) Introducing apis for gpt-3.5 turbo and whisper. Accessed: 2025-07-01. [Online]. Available: <https://openai.com/index/introducing-chatgpt-and-whisper-apis>
- [3] H. Touvron, L. Martin, K. Stone *et al.*, “Llama 2: Open foundation and fine-tuned chat models,” 2023. [Online]. Available: <https://arxiv.org/abs/2307.09288>
- [4] B. Hui, J. Yang, Z. Cui *et al.*, “Qwen2. 5-coder technical report,” *arXiv preprint arXiv:2409.12186*, 2024.
- [5] openai. (2025) Introducing gpt-5. Accessed: 2025-07-01. [Online]. Available: <https://openai.com/index/introducing-gpt-5>
- [6] meta. (2025) The llama 4 herd: The beginning of a new era of natively multimodal ai innovation. Accessed: 2025-07-01. [Online]. Available: <https://ai.meta.com/blog/llama-4-multimodal-intelligence>
- [7] J. Ribas. (2023) New bing. Accessed: 2025-07-01. [Online]. Available: <https://blogs.bing.com/search-quality-insights/february-2023/Building-the-New-Bing>
- [8] Google. (2025) Google gemini. Accessed: 2025-07-01. [Online]. Available: <https://blog.google/products/gemini>
- [9] Cursor. (2025) Cursor. Accessed: 2025-07-01. [Online]. Available: <https://cursor.com>
- [10] Y. Sun, S. Ma, T. Xiao *et al.*, “Accurate and Interpretable Log-Based Fault Diagnosis using Large Language Models,” *IEEE Transactions on Services Computing*, no. 01, pp. 1–14, Aug. 2025.
- [11] K. Team, Y. Bai, Y. Bao *et al.*, “Kimi k2: Open agentic intelligence,” 2025. [Online]. Available: <https://arxiv.org/abs/2507.20534>
- [12] Nvidia. (2022) Nvidia h100 tensor core gpu. Accessed: 2025-07-01. [Online]. Available: <https://www.nvidia.com/en-us/data-center/h100>
- [13] Z. Yao, Z. Tang, W. Yang *et al.*, “Enhancing LLM QoS Through Cloud-Edge Collaboration: A Diffusion-Based Multi-Agent Reinforcement Learning Approach,” *IEEE Transactions on Services Computing*, vol. 18, no. 03, pp. 1412–1427, May 2025.
- [14] Z. Li, W. Feng, M. Guizani *et al.*, “Tpi-llm: Serving 70b-scale llms efficiently on low-resource mobile devices,” *IEEE Transactions on Services Computing*, pp. 1–13, 2025.
- [15] Y. Li, J. Guo, Z. Tang *et al.*, “Cloud-Edge System for Scheduling Unpredictable LLM Requests with Combinatorial Bandit,” *IEEE Transactions on Services Computing*, no. 01, pp. 1–15, Sep. 2025.
- [16] T. Dao, D. Fu, S. Ermon *et al.*, “Flashattention: Fast and memory-efficient exact attention with io-awareness,” in *Advances in Neural Information Processing Systems*, vol. 35. Curran Associates, Inc., 2022, pp. 16 344–16 359.
- [17] R. A. Jacobs, M. I. Jordan, S. J. Nowlan *et al.*, “Adaptive mixtures of local experts,” *Neural Computation*, vol. 3, no. 1, pp. 79–87, 1991.
- [18] Y. Zhong, S. Liu, J. Chen *et al.*, “Distserve: disaggregating prefill and decoding for goodput-optimized large language model serving,” in *Proceedings of the 18th USENIX Conference on Operating Systems Design and Implementation*. USA: USENIX Association, 2024.
- [19] P. Patel, E. Choukse, C. Zhang *et al.*, “Splitwise: Efficient generative llm inference using phase splitting,” in *2024 ACM/IEEE 51st Annual International Symposium on Computer Architecture*, 2024, pp. 118–132.
- [20] M. Wang, Y. Ye, and Z. Zhou, “Llm serving optimization with variable prefill and decode lengths,” 2025. [Online]. Available: <https://arxiv.org/abs/2508.06133>
- [21] C. Hu, H. Huang, L. Xu *et al.*, “Shuffleinfer: Disaggregate llm inference for mixed downstream workloads,” *ACM Trans. Archit. Code Optim.*, vol. 22, no. 2, Jul. 2025. [Online]. Available: <https://doi.org/10.1145/3732941>
- [22] Nvidia. (2025) Nixl. Accessed: 2025-07-01. [Online]. Available: <https://github.com/ai-dynamo/nixl>
- [23] G.-I. Yu, J. S. Jeong, G.-W. Kim *et al.*, “Orca: A distributed serving system for Transformer-Based generative models,” in *16th USENIX Symposium on Operating Systems Design and Implementation*. Carlsbad, CA: USENIX Association, Jul. 2022, pp. 521–538.
- [24] W. Kwon, Z. Li, S. Zhuang *et al.*, “Efficient memory management for large language model serving with pagedattention,” in *Proceedings of the ACM SIGOPS 29th Symposium on Operating Systems Principles*, 2023.
- [25] A. Agrawal, N. Kedia, A. Panwar *et al.*, “Taming Throughput-Latency tradeoff in LLM inference with Sarathi-Serve,” in *18th USENIX Symposium on Operating Systems Design and Implementation*. Santa Clara, CA: USENIX Association, Jul. 2024, pp. 117–134.

- [26] A. K. Kamath, R. Prabhu, J. Mohan *et al.*, *POD-Attention: Unlocking Full Prefill-Decode Overlap for Faster LLM Inference*. NY, USA: Association for Computing Machinery, 2025, p. 897–912.
- [27] L. Zheng, L. Yin, Z. Xie *et al.*, “Sglang: efficient execution of structured language model programs,” in *Proceedings of the 38th International Conference on Neural Information Processing Systems*. NY, USA: Curran Associates Inc., 2024.
- [28] J. Yuan, H. Gao, D. Dai *et al.*, “Native sparse attention: Hardware-aligned and natively trainable sparse attention,” in *Proceedings of the 63rd Annual Meeting of the Association for Computational Linguistics (Volume 1: Long Papers)*. Vienna, Austria: Association for Computational Linguistics, Jul. 2025, pp. 23 078–23 097.
- [29] R. Qin, Z. Li, W. He *et al.*, “Mooncake: Trading more storage for less computation — a KVCache-centric architecture for serving LLM chatbot,” in *23rd USENIX Conference on File and Storage Technologies*. Santa Clara, CA: USENIX Association, Feb. 2025, pp. 155–170.
- [30] Y. Jin, T. Wang, H. Lin *et al.*, “P/d-serve: Serving disaggregated large language model at scale,” 2024. [Online]. Available: <https://arxiv.org/abs/2408.08147>
- [31] Y. Wu, T. Liu, Y. Zeng *et al.*, “Arrow: Adaptive scheduling mechanisms for disaggregated llm inference architecture,” 2025. [Online]. Available: <https://arxiv.org/abs/2505.11916>
- [32] Nvidia. (2025) ai-dynamo. Accessed: 2025-07-01. [Online]. Available: <https://github.com/ai-dynamo/dynamo>
- [33] G. E. P. Box and G. Jenkins, *Time Series Analysis, Forecasting and Control*. USA: Holden-Day, Inc., 1990.
- [34] J. Ribas. (2015) prometheus. Accessed: 2025-07-01. [Online]. Available: <https://github.com/prometheus/prometheus>
- [35] facebook. (2022) facebook/opt-30b. Accessed: 2025-07-01. [Online]. Available: <https://huggingface.co/facebook/opt-30b>
- [36] RedHatAI. (2025) Redhatai/deepseek-r1-distill-llama-70b-fp8-dynamic. Accessed: 2025-07-01. [Online]. Available: <https://huggingface.co/RedHatAI/DeepSeek-R1-Distill-Llama-70B-FP8-dynamic>
- [37] Y. Wang, Y. Chen, Z. Li *et al.*, “Burstgpt: A real-world workload dataset to optimize llm serving systems,” 2025. [Online]. Available: <https://arxiv.org/abs/2401.17644>
- [38] Microsoft. (2023) Azurepublicdataset. Accessed: 2025-07-01. [Online]. Available: <https://github.com/Azure/AzurePublicDataset>
- [39] anon8231489123. (2023) Sharegpt. Accessed: 2025-07-01. [Online]. Available: https://huggingface.co/datasets/anon8231489123/ShareGPT_Vicuna_unfiltered
- [40] Nvidia. (2025) Nvidia management library (nvm). Accessed: 2025-07-01. [Online]. Available: <https://developer.nvidia.com/management-library-nvm>



Junhan Liao received his bachelor’s degree in computer science and technology from Hunan University of Technology. Currently, he is a master’s student at Shenzhen Institutes of Advanced Technology, Chinese Academy of Sciences. His main research interests include large language models inference optimization and system management.



Award for Excellence (Early Career Award).

Minxian Xu (Senior Member, IEEE) is currently an Associate Professor at Shenzhen Institutes of Advanced Technology, Chinese Academy of Sciences. He received his PhD degree from the University of Melbourne in 2019. His research interests include resource scheduling and optimization in cloud computing. He has co-authored 80+ peer-reviewed papers published in prominent international journals and conferences. His PhD thesis was awarded the 2019 IEEE TCSC Outstanding Ph.D. Dissertation Award. He was also awarded the 2023 IEEE TCSC



Wanyi Zheng received her Bachelor’s degree from Hebei University in 2025. She is currently pursuing a Master’s degree at the Southern University of Science and Technology, and is also a joint-training student at the Shenzhen Institutes of Advanced Technology, Chinese Academy of Sciences. Her research interests include operating systems and the integration of large language model systems, with a primary focus on LLM inference optimization and system management.



Yan Wang (Member, IEEE) received the PhD degree in computer science from Inner Mongolia University, Hohhot, China, in 2015. She is currently an Associate Professor and a Master Supervisor of Computer Science and Technology with Inner Mongolia University. She has published more than 40 papers in international conferences and journals in her field. Her research interests include service computing, formal methods, and software technology.



cloud computing and network systems.

Kejiang Ye (Senior Member, IEEE) received the BSc and PhD degrees from Zhejiang University, in 2008 and 2013, respectively. He was also a joint PhD student with the University of Sydney from 2012 to 2013. After graduation, he works as post-doc researcher with Carnegie Mellon University from 2014 to 2015 and Wayne State University from 2015 to 2016. He is currently a professor with the Shenzhen Institutes of Advanced Technology, Chinese Academy of Sciences. His research interests focus on the performance, energy, and reliability of



ing worldwide (h-index=175, i10-index=837, 164,000+citations).

Rajkumar Buyya (Fellow, IEEE) is currently a Redmond Barry distinguished professor and director with the Quantum Cloud Computing and Distributed Systems (qCLOUDS) Laboratory, the University of Melbourne, Australia. He has authored more than 625 publications and seven textbooks including “Mastering Cloud Computing” published by McGraw Hill, China Machine Press, and Morgan Kaufmann for Indian, Chinese and international markets, respectively. He is one of the highly cited authors in computer science and software engineering



Chengzhong Xu (Fellow, IEEE) received the Ph.D. degree in computer science and engineering from the University of Hong Kong in 1993. He is the Dean of Faculty of Science and Technology and the Interim Director of Institute of Collaborative Innovation, University of Macau. He published two research monographs and more than 300 peer-reviewed papers in journals and conference proceedings. His papers received about 17K citations with an H-index of 72. His main research interests lie in parallel and distributed computing and cloud computing.